Available online at www.sciencedirect.com

ScienceDirect

Geochimica et Cosmochimica Acta 234 (2018) 84–97

Geochimica et Cosmochimica Acta

www.elsevier.com/locate/gca

Calibration and application of silica-water triple oxygen isotope thermometry to geothermal systems in Iceland and Chile

Jordan A.G. Wostbrock [a,*], Zachary D. Sharp [a], Camilo Sanchez-Yanez [b], Martin Reich [b], Daniela B. van den Heuvel [c,d], Liane G. Benning [c,e,f]

[a] University of New Mexico, Earth and Planetary Sciences, Albuquerque, NM, USA
[b] Department of Geology and Andean Geothermal Center of Excellence (CEGA), FCFM, Universidad de Chile, Santiago, Chile
[c] University of Leeds, School of Earth and Environment, Leeds, UK
[d] University of Bern, Institute of Geological Sciences, Bern, Switzerland
[e] German Research Center for Geosciences, GFZ, Potsdam, Germany
[f] Free University of Berlin, Department of Earth Sciences, Berlin, Germany

Received 18 September 2017; accepted in revised form 4 May 2018

Abstract

Triple oxygen isotope analyses were made on geothermal fluids and precipitates from Chile and Iceland to calibrate the silica-water isotopic fractionation for abiotic silica formation at elevated temperatures and were used to evaluate potential fractionation effects of biogenic vs. abiogenic samples and polymorphism. Coexisting water and amorphous silica precipitated inside the heat exchanger of the Hellisheiði power plant at 60 and 118 °C have triple oxygen isotope fractionations in excellent agreement with previous results from analyses of biogenic silica precipitated in cold waters.

In contrast to samples from the geothermal plant, natural amorphous silica precipitates and waters formed in active hot springs (T = 63–84 °C) in the Puchuldiza geothermal area of northern Chile gave temperature estimates from the silica-water thermometer far lower (37–46 °C) than the measured water temperatures. Active silica precipitation was found to only occur at and above the air-water interface on glass slides placed in the hot spring waters for 9 days. The calculated temperatures and visual inspection suggest that precipitation occurred along channel edges when saturation was overstepped by a factor of two. In contrast to the surficial neoformed amorphous silica, subsurface silica samples (>10 cm) have recrystallized to opal-CT and quartz within a sinter mound and these samples preserve isotope temperatures of 82 °C and 89 °C, in good agreement with the ambient temperatures of the thermal spring conduit system. The $\delta^{18}O$ values of abiogenic, low temperature silica formed in spring water far from the thermal waters with a measured temperature of 19 °C correspond to a silica-water temperature estimate of 20 °C. All samples preserved isotope data corresponding to their expected formation temperatures and appear to be in equilibrium in the triple oxygen isotope system. A best-fit θ–T relationship for silica-water using our inorganic silica-water samples is $\theta = 0.5305 - \frac{1.82(\pm 0.02)}{T(K)}$, $R^2 = 0.998$ $\left(\text{where } \theta_{a-b} = \frac{\ln \alpha^{17}O_{a-b}}{\ln \alpha^{18}O_{a-b}}\right)$. This new equation is indistinguishable from a previous empirical fit by Sharp et al. (2016) based primarily on biogenic silica samples, suggesting that the biogenic and abiogenic samples secreted silica with the same fractionation. Our results show that triple oxygen isotope measurements are robust and can be used

* Corresponding author at: Department of Earth and Planetary Sciences, University of New Mexico, 200 Yale Blvd, Albuquerque, NM 87131, USA.
E-mail address: jogibbons7@unm.edu (J.A.G. Wostbrock).

https://doi.org/10.1016/j.gca.2018.05.007

to estimate the temperature of formation, the isotopic composition of the formation water, and discern between equilibrium and non-equilibrium processes.

Keywords: Triple oxygen isotope fractionation; Silica solubility; Equilibrium fractionation; Quartz-water

1. INTRODUCTION

1.1. Geothermal Systems

Siliceous geothermal systems precipitate amorphous silica at the surface. The presence of siliceous springs indicates extensive water–rock interaction at depth. The maximum amount of dissolved silica in a fluid is controlled by quartz solubility when temperature is greater than 180 °C and chalcedony solubility for fluid temperatures below 110 °C (Arnórsson, 1975). As the geothermal spring water cools and becomes supersaturated, deposition of siliceous sinter (hereafter referred to as "sinter") occurs. Temperature is thought to be the main factor governing silica precipitation, while evaporation has an indirect effect by changing silica concentration in the fluid (e.g. Jones et al., 2000; Guidry and Chafetz, 2002; Mountain et al., 2003; Tobler et al., 2008; Nicolau et al., 2014). Sinter deposits can be composed of multiple silica phases including amorphous silica, opal cristobalite and/or cristobalite with tridymite (opal C/CT), and quartz (Herdianita et al., 2000; Campbell et al., 2001; Lynne and Campbell, 2003, 2004; Rodgers et al., 2004; Lynne et al., 2005, 2006, 2007, 2008; García-Valles et al., 2008; Nicolau et al., 2014). Initial deposition is always as amorphous silica while diagenesis to the crystalline, more stable, phases is thought to occur post-deposition with high-temperature fluid and/or steam (Lynne and Campbell, 2004). Sinter normally forms in near-neutral pH waters, with a high silica content, and variable anion and cation concentrations (Nicolau, 2013 and references therein) or as a residue of re-precipitated silica present in an acidic fumarole (White et al., 1956, Rodgers et al., 2004). Macroscopic silica textures are informally called lily pads, mounds (geyserite), rimming, terraces, and discharge aprons that are loosely related to temperature (Cady and Farmer, 1996; Lynne, 2012). Many of these textures are maintained even when the spring is no longer active and they can survive diagenesis (Lynne, 2012; Lynne and Campbell, 2004), making fossil sinter deposits (hereafter referred to as "paleosinter") an excellent resource for tracking hydrological conditions of the geothermal system. Similar to hot springs, precipitation of silica occurs inside geothermal power plants upon cooling of the water. These deposits are called silica scales and have been widely investigated due to their detrimental effect on the efficiency of geothermal energy production (e.g. Rothbaum et al., 1979; Harrar et al., 1982; Inagaki et al., 2003; Gunnarsson and Arnórsson, 2003, 2005; Padilla et al., 2005; Meier et al., 2014; Mroczek et al., 2017).

Both siliceous springs and geothermal power plants offer a unique site for the study of silica-water precipitation in terms of oxygen isotope fractionation. Geothermal power plants provide a controlled environment where the water flow and temperature are nearly constant, reducing the number of unconstrained variables when looking to calibrate or validate silica-water fractionation factors (Kita et al., 1985). Siliceous hot springs are natural systems that can be used to test the conditions at which silica precipitates in a natural setting. Many studies have looked at the $^{18}O/^{16}O$ ratio of geothermal water (e.g., Arnórsson, 1975; Giggenbach, 1978; Guidry and Chafetz, 2002; Geilert et al., 2015; Pope et al., 2010, 2016) or silica formed in geothermal water (e.g., Murata et al., 1977; Hayashi, 2013), but only two studies, to our knowledge, have measured both the water and the silica in either a geothermal power plant (Kita et al., 1985) or siliceous hot springs (Sharp et al., 2016). Geothermal systems have the potential to provide equilibrium isotope partitioning information over a temperature range that is difficult to duplicate in the laboratory (34–250 °C).

1.2. Triple oxygen isotope system

The $\delta^{17}O$ value of most terrestrial materials are about half the $\delta^{18}O$ value. A plot of $\delta^{17}O$ vs. $\delta^{18}O$ for rock samples plot with a slope of ~0.524 (Miller et al., 1999), whereas global meteoric waters plot with a slope of ~0.528 (Luz and Barkan, 2010). Waters with a $\delta^{18}O$ value greater than −10‰ plot with a slope of ~0.5275 (Luz and Barkan, 2010; Li et al., 2015; Sharp et al., 2016). The standard δ-notation (McKinney et al., 1950) to describe the isotopic abundance ratio of a sample is defined as

$$\delta^{x}O = \left(\frac{\left(\frac{^{x}O}{^{16}O}\right)_{sample}}{\left(\frac{^{x}O}{^{16}O}\right)_{VSMOW}} - 1 \right) \times 1000, \quad (1)$$

where x is either mass 17 or 18. A plot of $\delta^{18}O$ *vs.* $\delta^{17}O$ of terrestrial samples has a near perfect relationship with an R^2 value of 0.999 (Clayton, 1993; Rumble et al., 2007) and is called the Terrestrial Fractionation Line (TFL). Although deviations from the TFL can be tens of per mil in extraterrestrial samples (Clayton et al., 1973) or stratospheric samples resulting from mass-independent fractionation driven by photochemical reactions (Thiemens and Heidenreich, 1983), most natural materials follow the simple linear $\delta^{17}O$-$\delta^{18}O$ relationship with ±0.1‰. For most terrestrial geologic samples, the information provided by $\delta^{17}O$ values appears to add nothing to that obtained by $\delta^{18}O$ values alone. However, with improved analytical techniques, it is now recognized that subtle departures from the TFL exist in most terrestrial materials, and these departures can have geological significance such as formation temperatures and the extent of water–rock interaction (Pack and Herwartz, 2014; Herwartz et al., 2015).

The equilibrium fractionation of $\delta^{17}O$ between any two phases a and b is defined as:

$$\alpha^{17}O_{a-b} = (\alpha^{18}O_{a-b})^{\theta}, \quad (2)$$

where $\alpha_{a\text{-}b} = R_a/R_b$ and R is either $^{17}O/^{16}O$ or $^{18}O/^{16}O$ and θ ranges from 0.5 to 0.5305 for equilibrium or kinetic reactions (Cao and Liu, 2011). For systems where there is a 'crossover' such that $\delta'^{18}O_a - \delta'^{18}O_b = 0$, θ becomes undefined (Hayles et al., 2017). This phenomenon is not a concern for the silica-water system below temperatures of ~1000 °C (Sharp et al., 2016). Because of the relationship expressed in Eq. (2), the TFL has a slight curvature, which is removed when plotted in 'linearized notation' where:

$$\delta'O = 1000\ln\left(\frac{\delta}{1000} + 1\right). \quad (3)$$

The linearization of data allows us to directly compare variations over the full range of $\delta^{18}O$ values along a linear TFL (Hulston and Thode, 1965; Miller, 2002). By combining and rewriting the equilibrium fractionation equation with δ' notation, the mass-dependent equilibrium fractionation between two phases can be written as $1000\ln\alpha_{a\text{-}b} = \delta'^{x}O_a - \delta'^{x}O_b$ (where x is either mass 17 or 18). Variations above or below the TFL are expressed as $\Delta'^{17}O$, given by:

$$\Delta'^{17}O = \delta'^{17}O - \lambda \times \delta'^{18}O + \gamma. \quad (4)$$

λ is the reference slope and γ is the y-intercept. In this work, we use a λ value of 0.528 and a γ value of 0.0 to define $\Delta'^{17}O$.

While λ is used to describe the slope of the best fit, we use θ to describe processes controlled by equilibrium thermodynamics, defined for the triple oxygen isotope system as:

$$\theta_{a-b} = \frac{\delta'^{17}O_a - \delta'^{17}O_b}{\delta'^{18}O_a - \delta'^{18}O_b}, \quad (5)$$

where a and b are any two phases in equilibrium. A temperature dependence on θ was proposed theoretically (Urey, 1947; Matsuhisa et al., 1978; Young et al., 2002; Cao and Liu, 2011) and derived empirically for the silica-water mineral pair (Sharp et al., 2016). Cao and Liu (2011) calculated $\theta_{quartz\text{-}water}$ values over a temperature range of 0–100 °C. Their θ value of 0.5242 at 0 °C is slightly higher than the empirical estimate of 0.5237 ± 0.0001 based on biogenic silica samples (Sharp et al., 2016).

In kinetic oxygen isotopic fractionation, the λ of the $\delta'^{17}O$ and $\delta'^{18}O$ values of samples is closer to ~0.51, compared to ~0.52 of equilibrium processes. Biologic productivity such as respiration follows a kinetic slope of 0.518 (Luz and Barkan, 2005) while the slope of transpiration of leaf water varies between 0.5111–0.5204, depending on the humidity (Landais et al., 2006). Diffusion of water vapor in air follows a slope of 0.5185, resulting in the $\Delta^{17}O$ enrichment of meteoric water compared with marine (Barkan and Luz, 2007). The observed λ of kinetic processes differ from the calculated θ values of equilibrium processes and both provide a basis to determine whether the oxygen in geologic samples formed in equilibrium with their formation waters.

A number of experimental studies quantified the equilibrium oxygen isotope fractionation between quartz and water. A best fit compilation of the experimental and empirical data (Sharp et al., 2016) is given by

$$1000\ln\alpha^{18}_{SiO_2-water} = \frac{4.28\times10^6}{T^2} - \frac{3500}{T}, \quad (6)$$

where T is in Kelvin. Combining this equation with the empirical relationship for θ (Sharp et al, 2016), where

$$\theta_{SiO_2-water} = -\frac{1.85(\pm0.04)}{T(K)} + 0.5305,\ R^2 = 0.9998, \quad (7)$$

yields an equivalent silica-water equation for $\delta'^{17}O$:

$$1000\ln\alpha^{17}_{SiO_2-water} = \left(\frac{4.28\times10^6}{T^2} - \frac{3500}{T}\right) \times \left(0.5305 - \frac{1.85}{T}\right). \quad (8)$$

Eq. (6) can be rewritten in terms of the $\Delta'^{17}O$ values as:

$$\Delta'^{17}O_{SiO_2} - \Delta'^{17}O_{water} = \left(\frac{4.28\times10^6}{T^2} - \frac{3500}{T}\right) \times \left(0.5305 - \frac{1.85}{T} - \lambda_{RL}\right), \quad (9)$$

where λ_{RL} is an arbitrary reference slope as is taken as 0.528 in this study (Sharp et al., 2016). In the case where silica is in equilibrium with ocean water ($\delta^{17}O$ and $\delta^{18}O = 0‰$), the left side of Eq. (9) reduces to $\Delta'^{17}O_{SiO_2}$.

The silica-water triple oxygen isotope fractionation equations (Sharp et al., 2016) used a number of different sample types, including sinter and coexisting formation water in a siliceous hot spring from Yellowstone National Park, U.S.A, a marine chert sample, and silica from marine diatom frustules. The marine diatoms are of biogenic origin, leaving the question of any 'vital effect' unanswered. All samples used in the Sharp et al. (2016) single mineral thermometer were amorphous silica and it is unknown if the silica-water fractionation depends on crystallinity.

Here, we apply the silica-water triple oxygen isotope fractionation factors to silica and the formation water from the Puchuldiza hot springs in northern Chile and the Hellisheiði power plant in Iceland over the temperature range 19–118 °C. The triple oxygen isotope silica-water fractionation provides a rigorous test as to whether the silica in these geothermal systems formed via a kinetic process or in equilibrium with the formation water and the expected temperatures. The data are used to further refine the θ-T relationship for silica-water (Cao and Liu, 2011; Sharp et al., 2016) and explore whether biogenic silica precipitates in isotopic equilibrium with the formation water or shows a vital effect and if different silica polymorphs have different silica-water fractionations.

2. METHODS

2.1. Sampling

Silica and water samples were collected from the Hellisheiði geothermal plant, located about 25 km southeast of Reykjavik in southwest Iceland. The hydrothermal plant uses a 250–300 °C aquifer located at 2 km depth fed by meteoric water (Meier et al., 2014). Water is brought up

from depth and allowed to boil, the steam pressure being used to generate electricity. After steam separation, the hot fluid (118 °C) is passed through two heat exchangers, lowering the temperature to 60 °C, to produce thermal energy for district heating. The separated water is slightly alkaline with low salinity and a silica concentration of 758–795 ppm. The fluid is supersaturated with respect to amorphous silica, leading to silica scaling inside the pipelines and heat exchangers. To prevent precipitation from clogging wells or the reservoir, the water is combined with the steam condensate before being re-injected into the subsurface (Fig. 1).

Silica scale samples were retrieved from the heat exchangers during standard maintenance operations in January 2014. Six silica samples were collected: one from the inlet (118 °C ± 0.5; F.1), one from the outlet (60 °C ± 2.0; R.9), and four from chambers inside the heat exchanger with estimated temperatures of 100 °C, 85 °C, 75 °C, and 70 °C (F.2, F.3, R.10, R.5, respectively). Actual temperatures inside the heat exchanger are unknown. Silica samples were dried at 40 °C and stored in plastic containers. Water could only be sampled at the inlet (118 °C, 118 W) and outlet (60 °C, 60 W) of the heat exchanger. Water samples were stored in airtight containers and kept in a refrigerator to minimize evaporation.

The Puchuldiza hot springs are located in the Tarapacá Region of the Andean Cordillera, 160 km northwest of Iquique in northern Chile (S 19° 24′ 24.2″, W 068° 57′ 25.8″, Fig. 2). The geothermal field is about 1 km^2 and located at an elevation of 4200 meters above sea level (m. a.s.l). Temperatures of water at depth are estimated to be between 180 and 210 °C based on Na/K ratios and silica water content modeled with adiabatic expansion of hot water to the surface (Mahon and Cusicanqui, 1980; Lahsen et al., 2005; Tassi et al., 2010). The hot springs generally have temperatures near boiling at the surface expression (86.4 °C at 4200 m.a.s.l), although there are a few springs that have lower temperatures. The surficial geothermal water chemistry is slightly basic in pH (7.4–8.4), alkali-chloride type, with a silica content ranging from 227 to 400 ppm, near or above saturation (~300 ppm) with respect to amorphous silica at 85 °C (Gunnarsson and Arnórsson, 2000; Sanchez-Yanez et al., 2017). Sinter and water samples were collected in March 2016 in collaboration with the Andean Geothermal Center of Excellence (CEGA) at the University of Chile, Santiago.

Both silica and water were collected at various sites from the spring source and downstream at lower temperatures (Fig. 3). One low temperature (19 °C) silica sample (P13) and coexisting water (19.3 W) was obtained downstream of a geothermal spring where a thin sheet of silica was precipitating on the surface of the water over a layer of green algae (Fig. 3). To collect freshly precipitated silica, glass microscope slides were placed at three sites with water temperatures of 85 °C, 70 °C, and 63 °C (Fig. 3). Recently precipitated sinter was sampled (P63, P70, P84) by removing small sections of sinter exposed to the geothermal waters at each temperature location. Water temperature and pH were measured at each glass slide location in the afternoon on installation day, mid-morning on day 4, before sunrise on day 5 and in the afternoon on the removal day to evaluate the temperature variations of the spring during the silica precipitation period. Sinter that has undergone high-temperature recrystallization below the water's surface from springs was also sampled and labelled "paleosinter". Water was sampled at the time the plates were installed (63.2 W, 70.3 W, 84.6 W) and after the plates were removed, nine days later (62.3 W, 71.7 W, 81.4 W). Water was stored in 25 ml plastic bottles and refrigerated upon arrival at the University of New Mexico, Albuquerque, New Mexico, U.S.A.

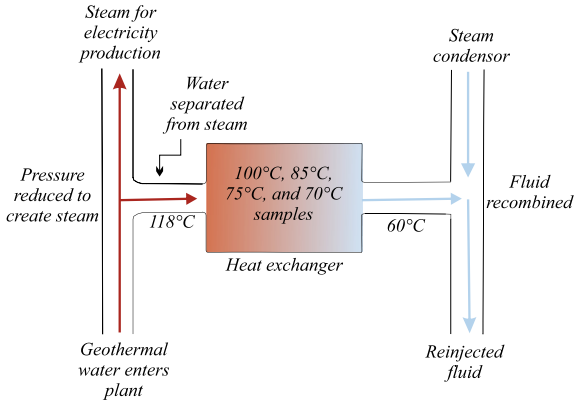

Fig. 1. Schematic of the heat exchanger of the Hellisheiði power plant in Iceland.

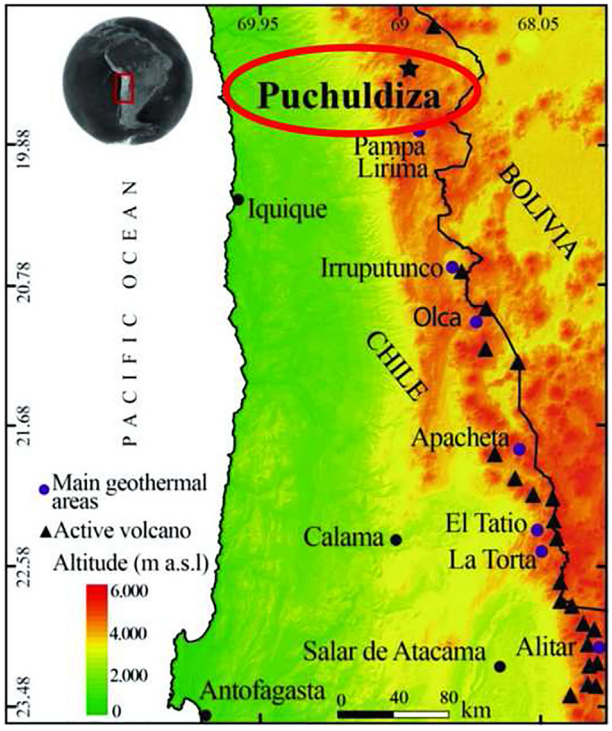

Fig. 2. Map of northern Chile showing the Puchulidza geothermal field in relation to cities of that region, volcanoes, and other geothermal areas (Image: Sanchez-Yanez et al., 2017).

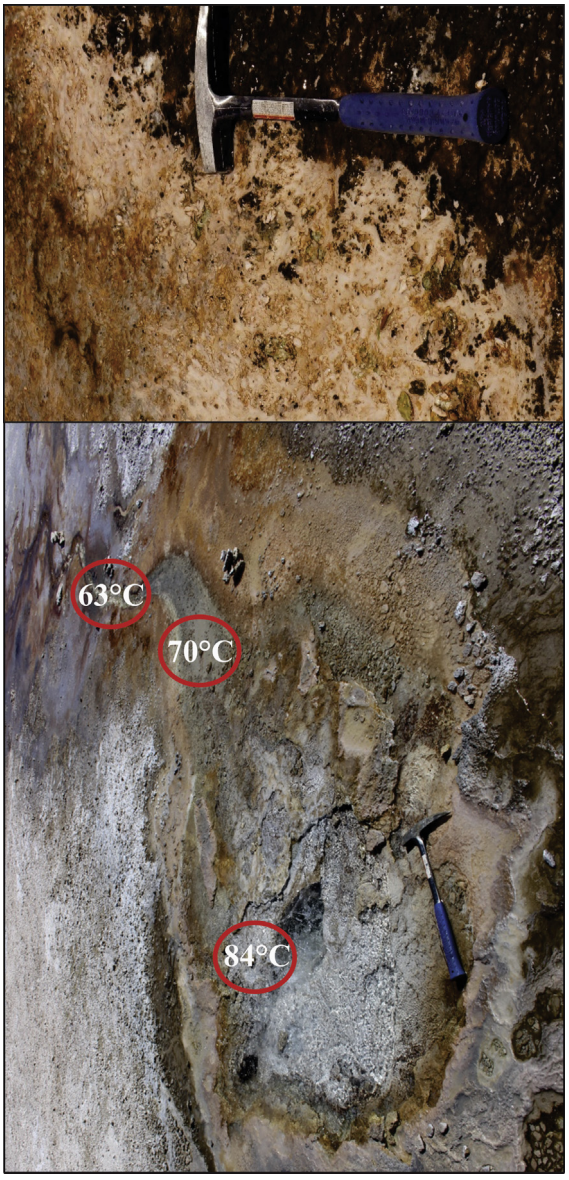

Fig. 3. Photographs of the hot spring pools at Puchuldiza (bottom). Red circles indicate locations of glass slides placed at the air–water interface for stable isotope analyses. Bubbling spring is 84.6 °C, boiling at the elevation of the geothermal field (4200 m. a.s.l). The photo on the top shows the 19 °C sample location site. The white layer is a thin, less than 2 mm, layer of abiogenic silica formed as a crust over green algae. (For interpretation of the references to color in this figure legend, the reader is referred to the web version of this article.)

2.2. Analysis

Silica samples were imaged and analyzed semi-qualitatively using a JEOL 82,000 SEM equipped with secondary electron, backscattered electron, and energy dispersive X-ray spectrometry detectors. Analytical conditions were an accelerating voltage of 15 kV and intensity of <1nA. Crystallinity was determined from powder X-ray diffraction. About 200 mg of each silica sample was analyzed using a Rigaku D/teX X-ray diffractometer. Jade® whole pattern fitting software was used for data analysis.

Silica samples were treated in 6 M HCl to remove carbonate prior to oxygen isotope analysis. Visible bubbling stopped after several hours. The samples were then rinsed with distilled water and dried at 60 °C. The oxygen isotope composition of the purified silica was measured using conventional laser fluorination (Sharp, 1990) with a GC column to separate traces of NF_3 gas. Samples were pre-fluorinated to remove any hydroxyl oxygen (Dodd and Sharp, 2010). Water was fluorinated for O_2 analysis by reacting a 1–2 μL aliquot of water with BrF_5 in a ¼ inch nickel tube for 4 min at ~150 °C as described in O'Neil and Epstein (1966). Water was also analyzed for $\delta^{18}O$ and δD using a Picarro L1102-I water isotopic analyzer.

The purified O_2 from each sample was analyzed with respect to the laboratory O_2 reference bottle calibrated relative to VSMOW, SLAP, NBS-28 and San Carlos olivine (see results in Sharp et al., 2016). Oxygen isotope analyses were made using a Thermo-Finnigan MAT 253 mass spectrometer. Each analysis consisted of a minimum of 30 iterations of 24 second integration time for both the sample and the standard to achieve $\Delta'^{17}O$ values with precision of ±0.005‰ (Luz and Barkan, 2010; Pack and Herwartz, 2014). All values are reported in per mil (‰) notation. Based on repeated analyses of our inhouse standards, the standard deviation (1σ) for $\delta^{17}O$, $\delta^{18}O$, and $\Delta^{17}O$ values are 0.05‰, 0.1‰, and 0.01‰. Theta values were calculated using the average $\delta'^{18}O$ and $\delta'^{17}O$ values of the geothermal water and corresponding silica samples following Eq. (5). A linear regression was performed to determine an equation for the best fit line using the data from this study, the data from Sharp et al. (2016), the combined data from this study and Sharp et al. (2016) and the data from Cao and Liu (2011). An ANOVA was performed to determine the 95% confidence interval of statistical significance between each data set.

3. RESULTS

All data are reported in Tables 1–3, A.1 and A.2. The $\delta^{18}O$, $\delta^{17}O$, and the respective linearized values ($\delta'^{18}O$, $\delta'^{17}O$) for

Table 1
Temperature and pH of each of the three sample sites from the Puchuldiza hot springs. Temperature and pH were measured at 4 separate times of day to track how temperature or pH may fluctuate daily.

	Day 1 (Plate Installation)				Day 4				Day 5				Day 9 (Plate Removal)			
	Time	Air T (°C)	Water T (°C)	pH	Time	Air T (°C)	Water T (°C)	pH	Time	Air T (°C)	Water T (°C)	pH	Time	Air T (°C)	Water T (°C)	pH
Site 1	3:30 PM	20.0	84.6	8.57	9:50 AM	14.1	82.3	8.55	7:15 AM	1.2	83.2	8.56	3:15 PM	18.1	81.4	8.68
Site 2	3:30 PM	20.0	70.3	8.80	9:50 AM	14.1	73.8	8.70	7:15 AM	1.2	72.9	8.64	3:15 PM	18.1	71.7	8.71
Site 3	3:30 PM	20.0	63.2	8.72	9:50 AM	14.1	64.8	8.72	7:15 AM	1.2	67.3	8.55	3:15 PM	18.1	62.3	8.67

Table 2
Data from the Hellisheiði Power Plant Compiled data of the water and silica samples from the Hellisheiði power plant in Iceland. All analyses were made at the Center for Stable Isotopes, University of New Mexico. All $\delta^{18}O$ and $\delta^{17}O$ values are reported relative to VSMOW. Bold numbers are the averages used in this study.

Sample	Sample Type	T (°C) Measured	δD	$\delta^{17}O$	$\delta^{18}O$	$\delta'^{17}O$	$\delta'^{18}O$	$\Delta'^{17}O$ (λ=0.528)	1000lnα ($^{17}O/^{16}O$)	1000lnα ($^{18}O/^{16}O$)	θ (Calc)	T (°C, Calc) $\delta'^{18}O$
118 W	Water	118	**−62.4**	−3.206	−6.045	−3.211	−6.063	−0.010				
				−3.545	−6.664	−3.551	−6.686	−0.021				
		Average		**−3.376**	**−6.355**	**−3.381**	**−6.375**	**−0.015**				
		±1σ		**(0.240)**	**(0.438)**	**(0.241)**	**(0.440)**	**(0.008)**				
60 W	Water	60	**−63.2**	−3.104	−5.847	−3.109	−5.864	−0.013				
				−3.162	−5.954	−3.167	−5.972	−0.014				
				−3.343	−6.295	−3.349	−6.315	−0.014				
		Average		**−3.203**	**−6.032**	**−3.208**	**−6.050**	**−0.014**				
		±1σ		**(0.125)**	**(0.234)**	**(0.125)**	**(0.235)**	**(0.001)**				
Average hot water value				**-3.289**	**−6.193**	**−3.295**	**−6.213**	**−0.014**				
± 1σ				**(0.176)**	**(0.326)**	**(0.177)**	**(0.328)**	**(0.004)**				
F.1	A. Silica[a]	118		6.830	13.091	6.807	13.006	−0.060				
				7.336	14.056	7.309	13.958	−0.061				
		Average		**7.083**	**13.573**	**7.058**	**13.482**	**−0.061**	**10.439**	**19.857**	**0.5257**	**111.3**
		±1σ		**(0.357)**	**(0.682)**	**(0.355)**	**(0.673)**	**(0.0005)**	**(0.397)**[b]	**(0.749)**	**(0.0004)**[c]	
F.2	A. Silica	100		8.687	16.655	8.649	16.518	−0.072				
				8.912	17.105	8.873	16.960	−0.083				
				9.267	17.774	9.224	17.618	−0.078				
				9.246	17.723	9.204	17.568	−0.072				
		Average		**9.028**	**17.314**	**8.987**	**17.166**	**−0.076**	**12.282**	**23.379**	**0.5254**	**86.4**
		±1σ		**(0.280)**	**(0.534)**	**(0.277)**	**(0.525)**	**(0.005)**	**(0.329)**	**(0.620)**	**(0.0004)**	
F.3	A. Silica	85		10.271	19.707	10.219	19.515	−0.085				
				10.346	19.845	10.293	19.651	−0.083				
				10.450	20.050	10.396	19.852	−0.086				
		Average		**10.356**	**19.867**	**10.302**	**19.673**	**−0.085**	**13.597**	**25.885**	**0.5253**	**71.5**
		±1σ		**(0.090)**	**(0.173)**	**(0.089)**	**(0.169)**	**(0.002)**	**(0.198)**	**(0.369)**	**(0.0004)**	
R.10	A. Silica	75		10.575	20.290	10.519	20.087	−0.086				
				10.411	19.949	10.357	19.753	−0.072				
				10.648	20.433	10.592	20.227	−0.088				
		Average		**10.545**	**20.224**	**10.489**	**20.022**	**−0.082**	**13.784**	**26.235**	**0.5254**	**69.5**
		±1σ		**(0.121)**	**(0.249)**	**(0.120)**	**(0.244)**	**(0.009)**	**(0.214)**	**(0.409)**	**(0.0004)**	
R.5	A. Silica	70		11.236	21.537	11.173	21.308	−0.077				
				10.950	21.026	10.890	20.808	−0.096				
		Average		**11.093**	**21.282**	**11.032**	**21.058**	**−0.087**	**14.327**	**27.271**	**0.5253**	**64.0**
		±1σ		**(0.202)**	**(0.361)**	**(0.200)**	**(0.354)**	**(0.013)**	**(0.267)**	**(0.483)**	**(0.0004)**	
R.9	A. Silica	60		11.345	21.766	11.281	21.533	−0.088				
				11.866	22.777	11.796	22.521	−0.095				
		Average		**11.606**	**22.272**	**11.539**	**22.027**	**−0.092**	**14.747**	**28.077**	**0.5252**	**59.9**
		±1σ		**(0.368)**	**(0.715)**	**(0.360)**	**(0.699)**	**(0.01)**	**(0.405)**	**(0.773)**	**(0.0004)**	

[a] "A-Silica" is Amorphous Silica.
[b] Error is root mean squared for 1000lnα values where $\sigma = \sqrt{\sigma^2_{silica} + \sigma^2_{water}}$.
[c] The θ error propagation is explained in Supplemental File.

each sample are reported in Tables 2 and 3. Measured and calculated temperatures are also reported for each sample. Detailed descriptions of each sample are in Table A.1.

4. DISCUSSION

4.1. Iceland

The $\delta^{18}O$ values of water throughout the geothermal heat exchanger are essentially constant (Supplementary Materials). The oxygen and hydrogen isotopic composition of the geothermal water agree with previous studies (Mutonga, 2007; Fig. 4). The 2–3‰ higher $\delta^{18}O$ values of the geothermal water compared to the local cold meteoric water of the region are probably due to steam release at the plant and/or hydrothermal exchange with the host basalt. The hydrogen isotope value of the water from the Hellisheiði power plant is nearly the same as the meteoric water of the region, as expected (Craig, 1963; Fig. 4). The triple oxygen isotopic compositions of the water samples

Table 3
Data from the Puchuldiza Geothermal System Compiled data of the water and silica samples from the Puchuldiza geothermal system in Chile. All analyses were made at the Center for Stable Isotopes, University of New Mexico. Bold numbers are the averages used in this study. All $\delta^{18}O$ and $\delta^{17}O$ values are reported relative to VSMOW.

Sample	Sample Type	T (°C) Measured	δD	$\delta^{17}O$	$\delta^{18}O$	$\delta'^{17}O$	$\delta'^{18}O$	$\Delta'^{17}O$ ($\lambda = 0.528$)	1000lnα ($^{17}O/^{16}O$)	1000lnα ($^{18}O/^{16}O$)	θ (Calc)	T (°C, Calc) $\delta'^{18}O$
19.3 W	Water	19.3	**−82.5**	−4.435	−8.394	−4.445	−8.429	0.006				
				−4.699	−8.890	−4.710	−8.930	0.005				
		Average		**−4.567**	**−8.642**	**−4.577**	**−8.680**	**0.005**				
		± 1σ		**(0.187)**	**(0.351)**	**(0.188)**	**(0.354)**	**(0.001)**				
63.2 W	Water	63.2		−6.158	−11.628	−6.177	−11.696	−0.001				
				−6.201	−11.694	−6.220	−11.763	−0.009				
62.3 W	Water	62.3	**−91.1**	−4.926	−9.287	−4.938	−9.330	−0.012				
		Average		**−5.762**	**−10.870**	**−5.779**	**−10.930**	**−0.008**				
		±1σ		**(0.030)**[a]	**(0.047)**[a]	**(0.031)**[a]	**(0.047)**[a]	**(0.006)**[a]				
70.3 W	Water	70.3	**−90.4**	−5.441	−10.263	−5.456	−10.316	−0.009				
71.7 W	Water	71.7	**−91.2**	−5.658	−10.672	−5.674	−10.729	−0.009				
		Average		**−5.550**	**−10.468**	**−5.565**	**−10.523**	**−0.009**				
		±1σ		**(0.153)**	**(0.289)**	**(0.154)**	**(0.292)**	**(0.000)**				
84.5 W	Water	84.5	**−92.1**	−5.671	−10.671	−5.687	−10.728	−0.023				
81.4 W	Water	81.4	**−92.7**	−5.222	−9.825	−5.236	−9.874	−0.022				
		Average		**−5.447**	**−10.248**	**−5.461**	**−10.301**	**−0.023**				
		±1σ		**(0.317)**	**(0.598)**	**(0.319)**	**(0.604)**	**(0.001)**				
Average hot spring value				**−5.586**	**−10.528**	**−5.602**	**−10.584**	**−0.013**				
± 1σ				**(0.616)**[b]	**(1.154)**[b]	**(0.619)**[b]	**(1.165)**[b]	**(0.010)**[b]				
P19	A. Silica[c]	19.3		15.299	29.454	15.183	29.029	−0.144				
				15.384	29.586	15.266	29.157	−0.128				
		Average		**15.341**	**29.520**	**15.225**	**29.093**	**−0.136**	**19.802**	**37.772**	**0.5243**	**20.3**
		±1σ		**(0.060**	**(0.093)**	**(0.059)**	**(0.091)**	**(0.011)**	**(0.197)**[d]	**(0.365)**[d]	**(0.0004)**[e]	
P63	A. Silica	63.2		11.287	21.688	11.224	21.456	−0.105				
				12.034	23.152	11.962	22.888	−0.123				
				12.146	23.369	12.073	23.100	−0.124				
				11.335	21.793	11.271	21.559	−0.112				
		Average		**11.701**	**22.500**	**11.633**	**22.251**	**−0.116**	**17.411**	**33.181**	**0.5247**	**37.1**
		±1σ		**(0.452)**	**(0.883)**	**(0.447)**	**(0.864)**	**(0.009)**	**(0.764)**	**(1.451)**	**(0.0004)**	
P70	A. Silica	70.3		11.762	22.698	11.693	22.444	−0.157				
				12.317	23.706	12.242	23.429	−0.129				
				11.409	21.897	11.344	21.661	−0.092				
		Average		**11.829**	**22.767**	**11.760**	**22.512**	**−0.126**	**17.325**	**33.034**	**0.5244**	**37.7**
		±1σ		**(0.458)**	**(0.906)**	**(0.452)**	**(0.886)**	**(0.032)**	**(0.767)**	**(1.464)**	**(0.0004)**	
Plate-70	A. Silica	70.3		10.977	21.085	10.917	20.866	−0.100				
				10.849	20.884	10.791	20.669	−0.123				
				10.621	20.434	10.565	20.228	−0.115				
		Average		**10.816**	**20.801**	**10.758**	**20.588**	**−0.113**	**16.323**	**31.110**	**0.5247**	**45.8**
		±1σ		**(0.180)**	**(0.333)**	**(0.178)**	**(0.327)**	**(0.012)**	**(0.644)**	**(1.210)**	**(0.0004)**	
P84	A. Silica	84.5		11.044	21.254	10.983	21.031	−0.121				
				12.122	23.342	12.049	23.074	−0.134				
				11.808	22.699	11.739	22.445	−0.112				
		Average		**11.658**	**22.432**	**11.591**	**22.184**	**−0.122**	**17.052**	**32.485**	**0.5249**	**39.9**
		±1σ		**(0.554)**	**(1.069)**	**(0.548)**	**(1.046)**	**(0.011)**	**(0.827)**	**(1.566)**	**(0.0004)**	
7a (Paleosinter)	Opal-CT	NA		7.131	13.726	7.106	13.633	−0.092				
				7.084	13.625	7.059	13.533	−0.086				
		Average		**7.108**	**13.676**	**7.082**	**13.583**	**−0.089**	**12.684**	**24.167**	**0.5248**	**81.5**
		±1σ		**(0.033)**	**(0.071)**	**(0.033)**	**(0.070)**	**(0.004)**	**(0.620)**	**(1.168)**	**(0.0004)**	
7b (Paleosinter)	Quartz	NA		6.493	12.483	6.472	12.406	−0.078				
				6.514	12.493	6.493	12.416	−0.063				
		Average		**6.504**	**12.488**	**6.482**	**12.411**	**−0.070**	**12.084**	**22.995**	**0.5255**	**88.8**
		±1σ		**(0.015)**	**(0.007)**	**(0.015)**	**(0.007)**	**(0.011)**	**(0.619)**	**(1.165)**	**(0.0004)**	

[a] The 62.3 W sample was not included in the standard deviation calculation.
[b] All water samples are used to calculate standard deviation.
[c] "A. Silica" is Amorphous Silica.
[d] Error is root mean squared for 1000lnα values where $\sigma = \sqrt{\sigma^2_{silica} + \sigma^2_{water}}$.
[e] The θ error propagation is explained in Supplemental File.

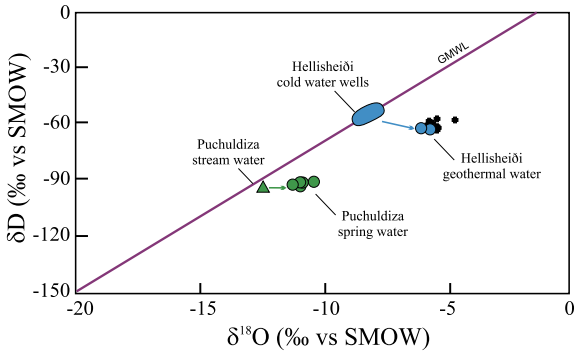

Fig. 4. Graph showing δD-$\delta^{18}O$ values of water from the Hellisheiði power plant and the Puchuldiza hot spring area. Blue ellipse shows that cold water wells (Mutonga, 2007) plot on the global meteoric water line (GMWL) while the hot water (small blue circles, this study and black crosses from Mutonga, 2007) have undergone water–rock interaction. Green triangle is cold, Puchuldiza stream water (Mahon and Cusicanqui, 1980) and plots near the GMWL while the hot spring water (green circle) shows some water–rock interaction. (For interpretation of the references to color in this figure legend, the reader is referred to the web version of this article.)

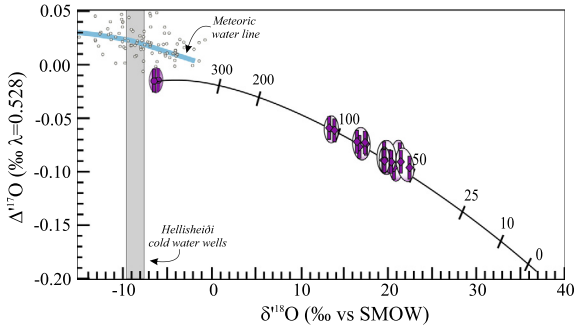

Fig. 5. $\Delta'^{17}O$-$\delta'^{18}O$ of the Icelandic sinter scale samples and thermal water along with a silica-water equilibrium curve fitted to an origin defined by the water values. Equilibrium temperatures are shown by tick marks intersecting the curve (Sharp et al., 2016). Diamonds are an individual analysis, error bars are the reported uncertainty, and the lighter circles group the data by sample.

plot within the range of currently measured meteoric waters (Luz and Barkan, 2010; Li et al., 2015; Sharp et al., 2016; Fig. 5). If high temperature interaction with basalt caused the $\delta^{18}O$ values of the water to increase (Hattori and Muehlenbachs, 1982), then the effective water/rock ratio can be calculated. The meteoric water near the Hellisheiði power plant has a $\delta^{18}O$ value of −8.0‰ to −9.0‰ (Mutonga, 2007) while the Icelandic bedrock (primarily Mid-Ocean Ridge Basalt, MORB, and hyaloclastites) has a $\delta^{18}O$ value of ~5‰ (Hattori and Muehlenbachs, 1982). Meteoric water has an average $\Delta'^{17}O$ value of 0.03‰ (Luz and Barkan, 2010) while mantle-derived materials are close to −0.05‰ (Sharp et al., 2016). Using a triple isotope mixing model (Herwartz et al., 2015), the water appears to be 20% altered after the high temperature exposure and rock interaction that the water experiences before the heat exchanger.

SEM and XRD analyses indicated that all silica samples were amorphous and SEM imaging showed a colloidal, globular texture (Fig. 6). The isotopic value of the silica increased from the 118 °C sample ($\delta'^{18}O = 13.5‰$, $\Delta'^{17}O = -0.061‰$) to the 60 °C sample ($\delta'^{18}O = 22.0‰$, $\Delta'^{17}O = -0.092‰$), consistent with a change in temperature of equilibration. Since the isotopic value of the water was constant throughout the heat exchanger, silica samples collected at all temperatures were assumed to be in equilibrium with water of the same isotopic composition.

Temperatures were estimated using Eqs. (6) and (8) and compared to the measured temperatures at the inlet (118 °C) and outlet (60 °C). The estimated temperatures using $\delta'^{17}O$ and $\delta'^{18}O$ values varied by less than 1 °C between Eqs. (6) and (8) and the relative error for the temperature estimate is ± 1.8 °C (Table 2). Using Eq. (9) to estimate temperatures result in a relative error of $^{+21}_{-17}$°C because a slight shift in $\Delta'^{17}O$ values equates to a larger temperature shift than when using $\delta'^{18}O$ or $\delta'^{17}O$ values alone. Eq. (9) is less useful for temperature estimates but is beneficial to see if samples are in equilibrium because there is a single solution for equilibrium using triple oxygen isotope values. All the silica samples satisfy the conditions of equilibrium with the formation water in $\Delta'^{17}O$-$\delta'^{18}O$ space (Fig. 5).

Temperature estimates from the silica-water fractionations agree very well with the measured temperatures at the 'high' and 'low' temperature sides of the heat exchanger (111.3 °C vs. 118 °C and 59.9 °C vs. 60 °C). Within the heat exchanger, temperature estimates from the silica-water fractionation are lower than the geothermal plant operator's estimates. Silica-water fractionation of silica precipitating in a geothermal plant in Japan was measured by Kita et al. (1985). The $1000\ln\alpha^{18}O_{silica\text{-}water}$ value of our 60 °C sample is only 0.13 higher than a sample collected at the same temperature in the Kita et al. (1985) study.

The θ-T variation from 60 to 118 °C is 0.0005, corresponding to a 0.00001 change in θ per °C over this temperature range. This is in excellent agreement with previous θ-T relationships (Cao and Liu, 2011; Sharp et al., 2016) for silica-water. The calculated θ values for the 118 °C and 60 °C samples are 0.5257 and 0.5252, respectively (Fig. 7). The best fit of the θ-T values of this study anchored at θ = 0.5305 at T = ∞, where T is in Kelvin, is:

$$\theta = -\frac{1.81(\pm 0.06)}{T} + 0.5305 \quad R^2 = 0.999. \tag{10}$$

Both an ANVOA (95% confidence interval) and the error on the coefficient in Eq. (10) is within analytical error of the θ-T relationship from Sharp et al. (2016) but is different than Cao and Liu (2011) ($P < 0.05$).

4.2. Chile

XRD analyses show that sinter samples from the active hot spring were amorphous silica while the paleosinter has recrystallized into opal-CT and microcrystalline quartz (Fig. 8). SEM imaging showed the 19.3 °C silica sample exhibited abiotic colloidal silica morphology even though it formed with green algae (Fig. 8). The quantitative XRD analysis of sample 7b showed a composition of

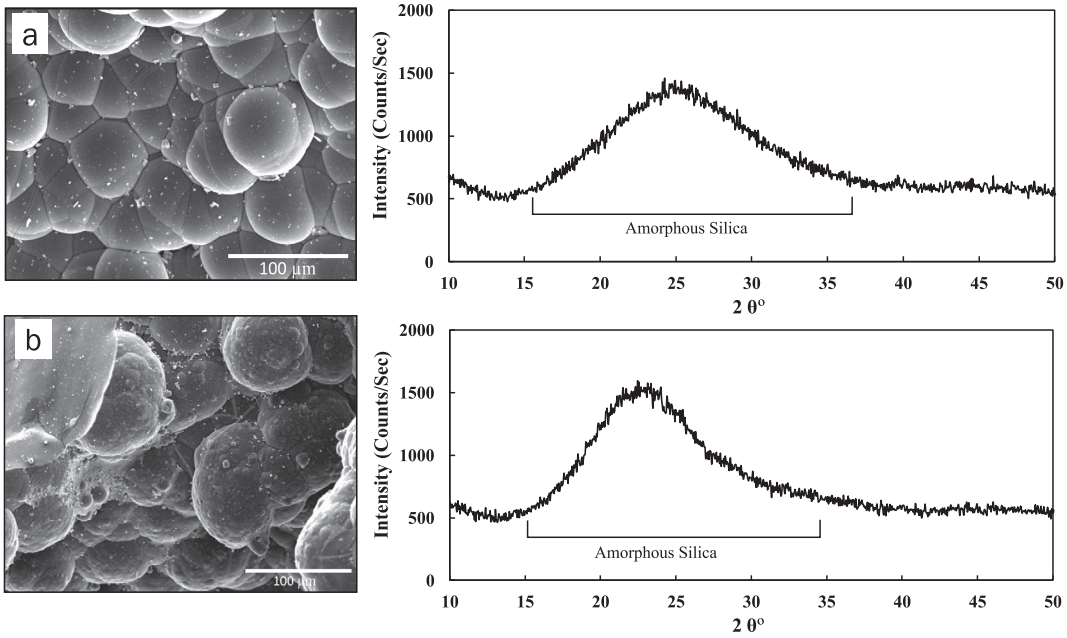

Fig. 6. SEM images (left) and XRD spectra (right) of sinter scale samples from the Hellisheiði power plant. (a) Sample of amorphous silica from the sample location corresponding to 118 °C (sample F.1). (b) Sample of amorphous silica from sample location corresponding to 60 °C (sample R.9). The XRD analyses show clear amorphous silica peaks.

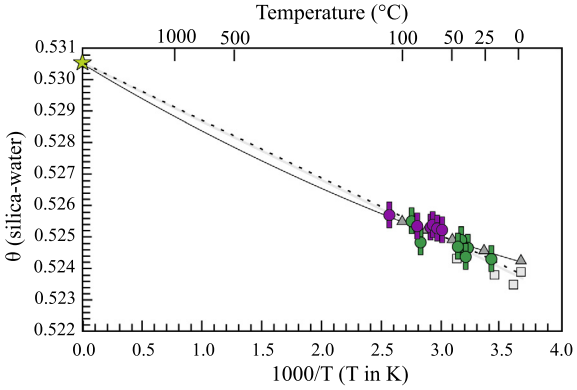

Fig. 7. Graph depicting measured θ vs temperature. Iceland samples (purple) are plotted using the measured temperatures for the 60 and 118 °C samples and the calculated temperatures for the remaining samples. Chile samples (green) are plotted using calculated temperatures from Eq. (6). Best fit using the whole dataset is the black dashed line. Also shown is θ-T relationships of Cao and Liu (2011, black curve) and Sharp et al. (2016, where light grey squares are measured data, and grey line is a best fit). (For interpretation of the references to color in this figure legend, the reader is referred to the web version of this article.)

97.8% quartz, 2.0% tridymite, and 0.2% calcite. Quantitative analysis of the surficial silica sample, P84, confirmed the crystallinity to be amorphous silica with 96.0% as amorphous, 3.8% as calcite, and only 0.2% as quartz. The quantitative analysis of sample 7a, taken mid-way from the surface and sample 7b of a paleospring, showed an intermediate silica crystallinity with 62.0% amorphous silica, 12.6% cristobalite, 11.4% calcite, 8.6% tridymite, and 5.6% quartz.

Neither temperature nor pH at each site varied by more than 5 °C and 0.2, respectively, over the 9 days of deployment (Table 1). Since pH does not appreciably affect silica solubility below a pH of 9.8 (Alexander et al., 1954), the pH variation is not responsible for silica precipitation. The $\delta^{18}O$ value of the hot spring waters plot about 2‰ heavier than the reported $\delta^{18}O$ value of meteoric water from a stream in the geothermal field (Mahon and Cusicanqui, 1980) but the δD values of both waters overlap with each other, indicating water–rock interaction in the geothermal field affected the oxygen but not hydrogen (Craig and Gordon, 1965; Mahon and Cusicanqui, 1980; Horita and Wesolowski, 1994; Fig. 4).

4.2.1. High temperature silica samples

Water samples from the hot spring showed similar $\delta^{18}O$ values regardless of temperature (Fig. 9, Table 3). Water from the spring source had an average $\delta'^{18}O$ value of −10.3‰ and varied by 0.85‰ between the first and last water sampling instance. The water sampled several meters from the source (around 63 °C) showed the largest variation in $\delta'^{18}O$ values with a 2.4‰ change between the first and last water sampling campaign, suggesting that evaporation may have affected these samples. However, the average $\delta'^{18}O$ value (−10.9‰) at the 63 °C location was similar to the other sampling sites (Fig. 9, Table 3). The $\Delta'^{17}O$ values of the water samples did not follow an evaporation trend, where the $\Delta'^{17}O$ values decrease with increasing evaporation. The average $\Delta'^{17}O$ values of hot spring waters were −0.023‰ at the source and −0.009‰ in the source's runoff channel (average of samples 63.2 W, 62.3 W, 70.3 W, and 71.7 W, Table 3).

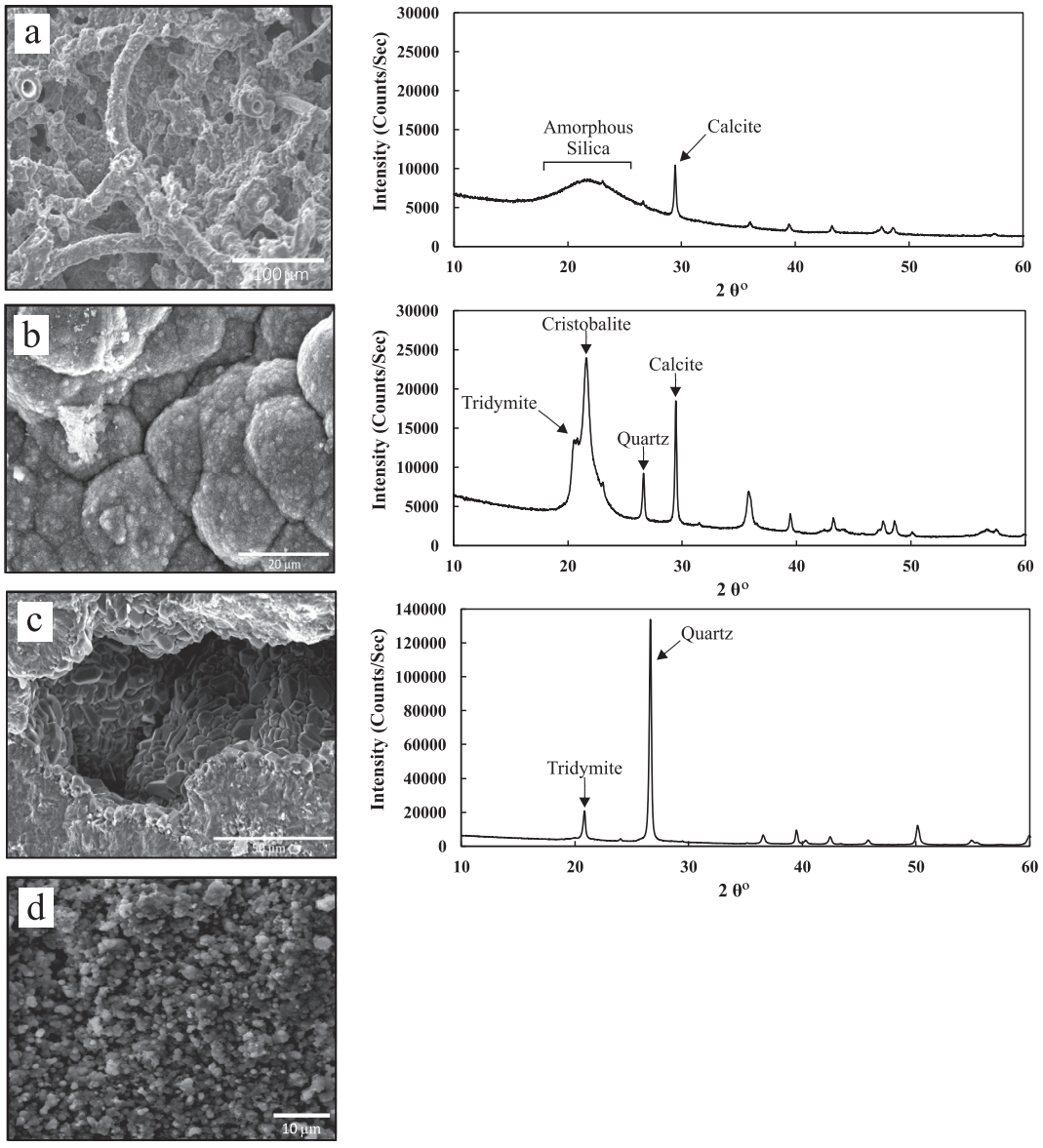

Fig. 8. SEM images (left) and corresponding XRD spectra (right) of sinter samples from the Puchuldiza geothermal field. (a) Sample P84. Silicified or coated microbes evident from SEM imagery. XRD spectra show amorphous silica as the predominant mineral. (b) Paleosinter sample 7a. The small platelets are Opal-CT, shown in the XRD spectra. (c) Paleosinter sample 7b depicting microcrystalline quartz growing in and around holes. The XRD spectra shows clear quartz peaks with very little contamination. (d) Abiogenic silica formed at 19.3 °C. All calcite was removed using HCl before isotopic analysis.

The isotopic values of surficial sinter samples from the active hot spring (samples P84, P70, P63, and Plate-70) plot on the silica-water equilibration trend with their formation waters, although the oxygen isotopic fractionations suggest formation temperatures of 37 to 46 °C, far lower than the measured water temperatures (Fig. 9). The lower calculated temperature estimates (Eq. (6)) suggest that the sinter either formed out of equilibrium with the water or is not precipitating at the temperature measured in the water but rather between 37 and 46 °C, driven by cooling and perhaps near-surface evaporation. The glass microscope slides that were left in the hot spring to collect fresh precipitation support this second hypothesis. No silica precipitation occurred on the slides below the surface of the water. Silica only precipitated at the air–water interface even though the waters are supersaturated (227–400 ppm) with respect to silica (Sanchez-Yanez et al., 2017; Table A.1). Silica precipitation at the air–water interface agree with the findings of Mountain et al. (2003), Tobler et al. (2008) and Nicolau et al. (2014) where hot spring waters that are slightly basic with saturation states ranging from undersaturated to supersaturated with respect to silica have low subaqueous precipitation and the primary driver of precipitation is evaporation and/or cooling.

The thermal waters from Chile are supersaturated with respect to amorphous silica but are not precipitating silica below the water surface of the hot springs. The calculated temperatures using isotope fractionation suggest that silica

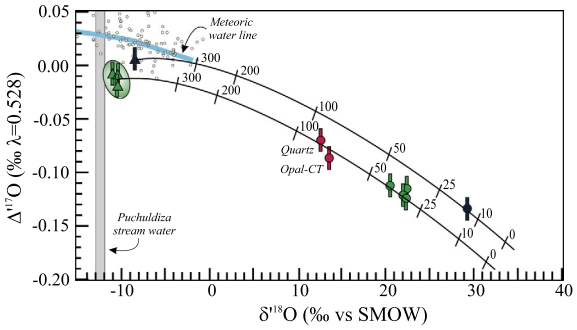

Fig. 9. $\Delta'^{17}O$-$\delta'^{18}O$ plot of Chilean sinter samples and thermal water with the single mineral thermometer fractionation line (Sharp et al., 2016). Silica and corresponding waters from near the thermal spring (green) plot on or very close to the fractionation line, with a presumed equilibrium precipitation at 37–46 °C. Red circles are the paleosinter samples that re-equilibrated at depth to microcrystalline quartz. These samples preserve the temperatures of the subsurface plumbing system. Dark blue triangle is the low temperature water and the dark blue circle is the corresponding silica. Error bars indicate the reported uncertainty. (For interpretation of the references to color in this figure legend, the reader is referred to the web version of this article.)

only precipitates when the waters cool to 38–46 °C. Visually this is supported because silica only formed above the air–water interface on the glass microscope slides and a build-up of sinter is seen along the edges of the outlet where splashing and overflow would occur. Therefore, the combined $\Delta'^{17}O$-$\delta'^{18}O$ oxygen isotope values of the precipitated sinter suggest that the silica formed in equilibrium with the fluid at 38–46 °C and in fluid containing up to almost double the silica concentration necessary for saturation (Gunnarsson and Arnórsson, 2000).

4.2.2. High temperature recrystallized samples

The subsurface sinter (paleosinter) recrystallized to a more stable silica polymorph and is more crystalline than the newly-precipitated surficial silica, consistent with post-burial recrystallization (Lynne et al., 2005). The $\Delta'^{17}O$-$\delta'^{18}O$ values of the paleosinter samples record temperatures that agree with the measured subsurface water temperatures. The triple oxygen isotope measurements of the paleosinter (samples 7a and 7b) suggest that the sinter re-equilibrated with the subsurface water close to the boiling point (Fig. 9). The paleosinter probably recrystallized in equilibrium below the surface at near-boiling conditions, preserving the highest temperature of the hot spring. The opal-CT sample (7a), found closer to the surface, suggests a lower temperature (81.5 °C) than the deeper, quartz paleosinter sample (7b, 88.8 °C). Most importantly, the $\Delta'^{17}O$-$\delta'^{18}O$ values of paleosinter samples 7a and 7b plot in equilibrium with the same water as the amorphous silica samples, reducing the possibility that polymorphism affects equilibrium isotope partitioning.

4.2.3. Low temperature sample

The low temperature silica (sample P19) appears to have formed in equilibrium with the coexisting water based on the combined $\Delta'^{17}O$-$\delta'^{18}O$ values (sample 19.3 W; Fig. 9). The measured and calculated temperatures are the same (19.3 °C measured vs. 20.5 ± 0.8 °C calculated). Texturally, the silica appears to be abiotic based on the SEM images (Fig. 8d). The θ value of 0.5242 is in agreement with the empirical estimate of Sharp et al. (2016) (0.5242) but lower than the theoretical estimate from Cao and Liu (2011) (0.5245). The Sharp et al. (2016) empirical estimate was determined mostly from biogenic silica samples (diatoms). The agreement between the biogenic and abiogenic results argues against a 'vital' effect for oxygen isotope fractionation during silica precipitation, and that diatoms secrete their silica frustules in isotopic equilibrium.

5. ICELAND VS. CHILE

Both the Iceland dataset and Chile dataset plot in equilibrium with the respective formation waters. In both sites, temperature drop, rather than evaporation, was the main driver for reaching silica supersaturation. The fluid within the heat exchanger in Iceland was already supersaturated with respect to silica and the silica precipitated at same temperature as the measured water. The springs in the Puchuldiza geothermal system are supersaturated with respect to silica, but given the strong temperature gradient at the fluid-air boundary, precipitation occurs predominantly at a temperature lower than the spring water temperatures. Recrystallized sinter a few centimeters below the surface preserves isotope fractionations close to boiling, suggesting that the silica undergoes recrystallization and reaches isotopic equilibrium with the subsurface fluid. Neither differences in pressure (9–10 bars in Iceland vs. ~0.7 bar in Chile), flow (~420 L/s in Iceland vs. fast/intermittent flow in Chile), or salt content ($[Na^+]$,$[Cl^-] = 194$ ppm, 166 ppm in Iceland vs. 1520 ppm, 2404 ppm in Chile) had any noticeable effect on oxygen isotope partitioning (Table A.2), in agreement with previous studies (Sharp, 2017).

6. A GENERALIZED θ-T RELATIONSHIP FOR SILICA-WATER

All theta calculations of this study were closer to ~0.524 and not lower, as would be expected from kinetic processes, and are interpreted to form in equilibrium with its formation waters. A best-fit θ-T relationship for inorganic silica-water can be made using the Iceland and Chile data. The measured temperatures of the two Iceland samples are included in our best fit. The measured and estimated temperatures using the silica-water isotope thermometer (Eq. (6)) for these two samples are in excellent agreement. The remaining Iceland samples are included using the calculated temperatures (Eq. (6)). All samples from Chile were used for the best-fit θ-T relationship using temperatures estimated from the $\delta^{18}O$ silica-water oxygen isotope thermometer (Eq. (6)). Using the data from this study, an overall inorganic silica-water θ-T relationship is given by:

$$\theta = 0.5305 - \frac{1.82(\pm 0.02)}{T(K)} \quad R^2 = 0.998 \text{ where,}$$

$$\theta_{a-b} = \frac{\ln \alpha^{17}O_{a-b}}{\ln \alpha^{18}O_{a-b}}. \tag{11}$$

This new equation is indistinguishable from a previous empirical fit by Sharp et al. (2016) ($P > 0.05$) based primarily on biogenic silica samples, suggesting that silica in biogenic and abiogenic samples was formed with the same oxygen isotope fractionation. Combining the data from this study with the predominately biogenic silica samples from Sharp et al. (2016) yields a silica-water θ-T relationship given by:

$$\theta = 0.5305 - \frac{1.84(\pm 0.02)}{T(K)} \quad R^2 = 0.998. \tag{12}$$

7. CONCLUSION

The triple oxygen isotope values of silica scale and coexisting water from the geothermal plant in Iceland as well as a low temperature sample from Chile allow us to refine the θ-T relationship. Paired $\delta'^{17}O$-$\delta'^{18}O$ measurements can be used to accurately estimate the temperature of formation, the isotopic composition of the formation water, and most importantly, discern between equilibrium and non-equilibrium processes. Based on the samples from the geothermal plant and the Chilean hot springs, it appears that the oxygen isotope silica-water fractionation factors are equally valid for amorphous silica, opal CT and quartz. There does not appear to be any appreciable difference in the fractionation of water with either abiogenic or biogenic silica. The triple oxygen isotope system suggests the subsurface sinter re-equilibrated with the hydrothermal water at Puchuldiza during recrystallization and preserves the near-boiling temperature of the hot spring. Natural systems, such as geothermal fields, provide an excellent resource for further exploration on the effects that evaporation and temperature have on the triple oxygen isotope system and equilibrium silica-water fractionation.

ACKNOWLEDGEMENTS

Jordan Wostbrock acknowledges support from the United States National Science Foundation Grant # DGE-1418062. We thank the thoughtful and constructive reviews of Issaku Kohl, Andreas Pack, and Justin Hayles. We thank E. Gunnlaugsson and H. Bergmann for assisting with the collection of silica scales and fluid samples at the Hellisheiði power plant. Daniela van den Heuvel would like to acknowledge the financial support by the Marie Curie grant from the European Commission in the framework of the MINSC Initial Training Research network, Project number 290040 and the 2014 PhD Student Grant by the International Geothermal Association (IGA). Martin Reich acknowledges support from FONDAP-CONICYT project 15090013 "Andean Geothermal Center of Excellence (CEGA)" and from Millennium Nucleus for Metal Tracing Along Subduction (NMTM), MSI Grant NC130065.

APPENDIX A. SUPPLEMENTARY MATERIAL

Supplementary data associated with this article can be found, in the online version, at https://doi.org/10.1016/j.gca.2018.05.007.

REFERENCES

Alexander G. B., Heston W. M. and Iler R. K. (1954) The solubility of amorphous silica in water. *J. Phys. Chem.* **58**, 453–455.

Arnorsson S. (1975) Application of silica geothermometer in low-temperature hydrothermal areas in Iceland. *Am. J. Sci.* **275**, 763–784.

Barkan L. and Luz B. (2007) Diffusivity fractionations of H216O/H217O and H216O/ H218O in air and their implications for isotope hydrology. *Rapid Commun. Mass Spectrom.* **21**, 2999–3005.

Cady S. L. and Farmer J. D. (1996) Fossilization processes in siliceous thermal springs: Trends in reservation along thermal gradients. In *Evolution of Hydrothermal Ecosystems on Earth* (eds. G. R. Bock and J. A. Goode). John Wiley & Sons Ltd, Chichester, pp. 150–173.

Campbell K. A., Sannazzaro K., Rodgers K. A., Herdianita N. R. and Browne P. R. L. (2001) Sedimentary facies and mineralogy of the late Pleistocene Umukuri silica sinter, Taupo Volcanic Zone, New Zealand. *J. Sediment. Res.* **71**, 727–746.

Cao X. B. and Liu Y. (2011) Equilibrium mass-dependent fractionation relationships for triple oxygen isotopes. *Geochim. Cosmochim. Acta* **75**, 7435–7445.

Clayton R. N. (1993) Oxygen isotopes in meteorites. *Annu. Rev. Earth Planet. Sci.* **21**, 115–149.

Clayton R. N., Grossman L. and Mayeda T. K. (1973) Component of primitive nuclear composition in carbonaceous meteorites. *Science* **182**, 485–488.

Craig H. (1963) The isotopic geochemistry of water and carbon in geothermal areas. Nuclear Geology on Geothermal Areas. Spoleto, Italy, pp. 17–53.

Craig H. and Gordon L.I. (1965) Deuterium and oxygen 18 variations in the ocean and the marine atmosphere. In Stable Isotopes in Oceanographic Studies and Paleotemperatures (ed. E. Tongiorgi). Spoleto, pp. 9–130.

Dodd J. P. and Sharp Z. D. (2010) A laser fluorination method for oxygen isotope analysis of biogenic silica and a new oxygen isotope calibration of modern diatoms in freshwater environments. *Geochim. Cosmochim. Acta* **74**, 1381–1390.

Garcia-Valles M., Fernandez-Turiel J. L., Gimeno-Torrente D., Saavedra-Alonso J. and Martinez-Manent S. (2008) Mineralogical characterization of silica sinters from the El Tatio geothermal field, Chile. *Am. Miner.* **93**, 1373–1383.

Geilert S., Vroon P. Z., Keller N. S., Gudbrandsson S., Stefansson A. and van Bergen M. J. (2015) Silicon isotope fractionation during silica precipitation from hot-spring waters: Evidence from the Geysir geothermal field, Iceland. *Geochim. Cosmochim. Acta* **164**, 403–427.

Giggenbach W. F. (1978) The isotopic composition of waters from the El Tatio geothermal field, Northern Chile. *Geochim. Cosmochim. Acta* **42**, 979–988.

Guidry S. A. and Chafetz H. S. (2002) Factors governing subaqueous siliceous sinter precipitation in hot springs: examples from Yellowstone National Park, USA. *Sedimentology* **49**, 1253–1267.

Gunnarsson I. and Arnórsson S. (2000) Amorphous silica solubility and the thermodynamic properties of H_4SiO_4 in the range of 0° to 350°C at Psat. *Geochim. Cosmochim. Acta* **64**, 2295–2307.

Gunnarsson I. and Arnorsson S. (2005) Treatment of geothermal waste water to prevent silica scaling. World Geothermal Congress, Antalya, Turkey, pp. 1–5.

Gunnarsson I. and Arnórsson S. (2003) Silica scaling: The main obstacle in efficient use of high-temperature geothermal fluids. International Geothermal Conference, Reykjavik, Iceland, pp. 30–36.

Harrar J. E., Locke F. E., Otto C. H., Lorensen L. E., Monaco S. B. and Frey W. P. (1982) Field-tests of organic additives for scale control at the Salton-sea geothermal-field. *Soc. Petrol. Eng. J.* **22**, 17–27.

Hattori K. and Muehlenbachs K. (1982) Oxygen isotope ratios of the Icelandic crust. *J. Geophys. Res.* **87**, 6559–6565.

Hayashi K. (2013) Oxygen isotope study of silica sinter from the Osorezan geothermal field, northeast Japan. *Int. J. Geosci.* **4**, 1438–1446.

Hayles J. A., Cao X. and Bao H. (2017) The statistical mechanical basis of the triple isotope fractionation relationship. *Geophys. Res. Lett.* **3**, 1–11.

Herdianita N. R., Browne P. R. L., Rodgers K. A. and Campbell K. A. (2000) Mineralogical and textural changes accompanying ageing of silica sinter. *Miner. Depos.* **35**, 48–62.

Herwartz D., Pack A., Krylov D., Xiao Y. L., Muehlenbachs K., Sengupta S. and Di Rocco T. (2015) Revealing the climate of snowball Earth from Delta O-17 systematics of hydrothermal rocks. *Proc. Natl. Acad. Sci. U. S. A.* **112**, 5337–5341.

Horita J. and Wesolowski D. J. (1994) Liquid-vapor fractionation of oxygen and hydrogen isotopes of water from the freezing to the critical-temperature. *Geochim. Cosmochim. Acta* **58**, 3425–3437.

Hulston J. R. and Thode H. G. (1965) Variations in the 33S, 34S, and 36S contents of meteorites and their relation to chemical and nuclear efforts. *J. Geophys. Res.* **70**, 3475–3484.

Inagaki F., Motomura Y. and Ogata S. (2003) Microbial silica deposition in geothermal hot waters. *Appl. Microbiol. Biotechnol.* **60**, 605–611.

Jones B., Renaut R. W. and Rosen M. R. (2000) Stromatolites forming in acidic hot-spring waters, North Island, New Zealand. *Palaios* **15**, 450–475.

Kita I., Taguchi S. and Matsubaya O. (1985) Oxygen isotope fractionation between amorphous silica and water at 34–93 degrees C. *Nature* **314**, 83–84.

Lahsen A., Sepúlveda F., Rojas J. and Palacios C. (2005) Present status of geothermal exploration in Chile. World Geothermal Congress, Antalya, Turkey, pp. 1–9.

Landais A., Barkan E., Yakir D. and Luz B. (2006) The triple oxygen isotopic composition of oxygen in leaf water. *Geochim. Cosmochim. Acta.* **70**, 4105–4115.

Li S., Levin N. E. and Chesson L. A. (2015) Continental scale variation in 17O-excess of meteoric waters in the United States. *Geochim. Cosmochim. Acta* **164**, 110–126.

Luz B. and Barkan E. (2005) The isotopic ratios 17O/16O and 18O/16O in molecular oxygen and their significance in biogeochemistry. *Geochim. Cosmochim. Acta* **69**, 1099–1110.

Luz B. and Barkan E. (2010) Variations of O-17/O-16 and O-18/O-16 in meteoric waters. *Geochim. Cosmochim. Acta* **74**, 6276–6286.

Lynne B. Y. (2012) Mapping vent to distal-apron hot spring paleoflow pathways using siliceous sinter architecture. *Geothermics* **43**, 3–24.

Lynne B. Y. and Campbell K. A. (2003) Diagenetic transformations (opal-A to quartz) of low- and mid-temperature microbial textures in siliceous hot-spring deposits, Taupo Volcanic Zone, New Zealand. *Can. J. Earth Sci.* **40**, 1679–1696.

Lynne B. Y. and Campbell K. A. (2004) Morphologic and mineralogic transitions from opal-A to opal-CT in low-temperature siliceous sinter diagenesis, Taupo Volcanic Zone, New Zealand. *J. Sediment. Res.* **74**, 561–579.

Lynne B. Y., Campbell K. A., James B. J., Browne P. R. L. and Moore J. (2007) Tracking crystallinity in siliceous hot-spring deposits. *Am. J. Sci.* **307**, 612–641.

Lynne B. Y., Campbell K. A., Moore J. and Browne P. R. L. (2008) Origin and evolution of the Steamboat Springs siliceous sinter deposit, Nevada, USA. *Sediment. Geol.* **210**, 111–131.

Lynne B. Y., Campbell K. A., Moore J. N. and Browne P. R. L. (2005) Diagenesis of 1900-year-old siliceous sinter (opal-A to quartz) at Opal Mound, Roosevelt Hot Springs, Utah, USA. *Sediment. Geol.* **179**, 249–278.

Lynne B. Y., Campbell K. A., Perry R. S., Browne P. R. L. and Moore J. N. (2006) Acceleration of sinter diagenesis in an active fumarole, Taupo volcanic zone, New Zealand. *Geology* **34**, 749–752.

Mahon W. A. J. and Cusicanqui H. (1980) Geochemistry of the Puchuldiza and Tuja hot springs, Chile. *NZ J. Sci.* **23**, 149–159.

Matsuhisa Y., Goldsmith J. R. and Clayton R. N. (1978) Mechanisms of hydrothermal crystallization of quartz at 250 degrees C and 15 kbar. *Geochim. Cosmochim. Acta* **42**, 173–182.

McKinney C. R., McCrea J. M., Epstein S., Allen H. A. and Urey H. C. (1950) Improvements in mass spectrometers for the measurement of small differences in isotope abundance ratios. *Rev. Sci. Instrum.* **21**, 724–730.

Meier D. B., Gunnlaugsson E., Gunnarsson I., Jamtveit B., Peacock C. L. and Benning L. G. (2014) Microstructural and chemical variation in silica-rich precipitates at the Hellisheidi geothermal power plant. *Mineral. Mag.* **78**, 1381–1389.

Miller M. F. (2002) Isotopic fractionation and the quantification of O-17 anomalies in the oxygen three-isotope system: an appraisal and geochemical significance. *Geochim. Cosmochim. Acta* **66**, 1881–1889.

Miller M. F., Franchi I. A., Sexton A. S. and Pillinger C. T. (1999) High precision delta O-17 isotope measurements of oxygen from silicates and other oxides: Method and applications. *Rapid Commun. Mass Spectrom.* **13**, 1211–1217.

Mountain B. W., Benning L. G. and Boerema J. A. (2003) Experimental studies on New Zealand hot spring sinters: rates of growth and textural development. *Can. J. Earth Sci.* **40**, 1643–1667.

Mroczek E., Graham D., Siega C. and Bacon L. (2017) Silica scaling in cooled silica saturated geothermal water: Comparison between Wairakei and Ohaaki geothermal fields, New Zealand. *Geothermics* **69**, 145–152.

Murata K. J., Friedman I. and Gleason J. D. (1977) Oxygen isotope relations between diagenetic silica minerals in Monterey Shale, Temblor Range, California. *Am. J. Sci.* **277**, 259–272.

Mutonga M. (2007) The isotopic and chemical characteristics of geothermal fluids in Hengill area, SW-Iceland: Hellisheidi, Hveragerdi and Nesjavellir fields, Geothermal Training Programme. United Nations University, Reykjavik, Iceland, pp. 333–370.

Nicolau C. (2013) Physico-Chemical and Environmental Controls on Siliceous Sinter Formation at the High-Altitude El Tatio Geothermal Field, Northern Chile. M.S Thesis: Universidad de Chile, 45 p.

Nicolau C., Reich M. and Lynne B. (2014) Physico-chemical and environmental controls on siliceous sinter formation at the high-altitude El Tatio geothermal field, Chile. *J. Volcanol. Geotherm. Res.* **282**, 60–76.

O'Neil J. R. and Epstein S. (1966) A method for oxygen isotope analysis of milligram quantities of water and some of its applications. *J. Geophys. Res.* **71**, 4955–4961.

Pack A. and Herwartz D. (2014) The triple oxygen isotope composition of the Earth mantle and understanding Delta O-17 variations in terrestrial rocks and minerals. *Earth Planet. Sci. Lett.* **390**, 138–145.

Padilla S. R. M., Barnett P., Castro M., Guerra E. and Henríquez J. L. (2005) Silica Polymerization and Deposition Trials at the Berlin Geothermal Field, El Salvador. World Geothermal Congress, Antalya, Turkey, pp. 1–4.

Pope E., Bird D. K., Arnórsson S., Fridriksson T., Elders W. A. and Fridleifsson G. O. (2010) Iceland Deep Drilling Project

(IDDP): Stable Isotope Evidence of Fluid Evolution in Icelandic Geothermal Systems. World Geothermal Congress, Bali, Indonesia, pp. 1–7.

Pope E. C., Bird D. K., Arnorsson S. and Giroud N. (2016) Hydrogeology of the Krafla geothermal system, northeast Iceland. *Geofluids* **16**, 175–197.

Rodgers K. A., Browne P. R. L., Buddle T. F., Cook K. L., Greatrex R. A., Hampton W. A., Herdianita N. R., Holland G. R., Lynne B. Y., Martin R., Newton Z., Pastars D., Sannazarro K. L. and Treece C. I. A. (2004) Silica phases in sinters and residues from geothermal fields of New Zealand. *Earth-Sci. Rev.* **66**, 1–61.

Rothbaum H. P., Anderton B. H., Harrison R. F., Rohde A. G. and Slatter A. (1979) Effect of silica polymerisation and pH on geothermal scaling. *Geothermics* **8**, 1–20.

Rumble D., Miller M. F., Franchi I. A. and Greenwood R. C. (2007) Oxygen three-isotope fractionation lines in terrestrial silicate minerals: An inter-laboratory comparison of hydrothermal quartz and eclogitic garnet. *Geochim. Cosmochim. Acta* **71**, 3592–3600.

Sanchez-Yanez C., Reich M., Leisen M., Morata D. and Barra F. (2017) Geochemistry of metals and metalloids in siliceous sinter deposits: Implications for elemental partitioning into silica phases. *Appl. Geochem.* **80**, 112–133.

Sharp Z. D. (1990) A laser-based microanalytical method for the in situ determination of oxygen isotope ratios of silicates and oxides. *Geochim. Cosmochim. Acta* **54**, 1353–1357.

Sharp Z. D. (2017) Principles of Stable Isotope Geochemistry, 2nd ed.

Sharp Z. D., Gibbons J. A., Maltsev O., Atudorei V., Pack A., Sengupta S., Shock E. L. and Knauth L. P. (2016) A calibration of the triple oxygen isotope fractionation in the SiO_2-H_2O system and applications to natural samples. *Geochim. Cosmochim. Acta* **186**, 105–119.

Tassi F., Aguilera F., Darrah T., Vaselli O., Capaccioni B., Poreda R. J. and Huertas A. D. (2010) Fluid geochemistry of hydrothermal systems in the Arica-Parinacota, Tarapaca and Antofagasta regions (northern Chile). *J. Volcanol. Geotherm. Res.* **192**, 1–15.

Thiemens M. H. and Heidenreich J. E. (1983) The mass-independent fractionation of oxygen: a novel isotope effect and its possible cosmochemical implications. *Science* **219**, 1073–1075.

Tobler D. J., Stefánsson A. and Benning L. G. (2008) In-situ grown silica sinters in Icelandic geothermal areas. *Geobiology* **6**, 481–502.

Urey H. C. (1947) The thermodynamic properties of isotopic substances. *J. Chem. Soc.*, 562–581.

White D. E., Brannock W. W. and Murata K. J. (1956) Silica in hot-spring waters. *Geochim. Cosmochim. Acta* **10**, 27–59.

Young E. D., Galy A. and Nagahara H. (2002) Kinetic and equilibrium mass-dependent isotope fractionation laws in nature and their geochemical and cosmochemical significance. *Geochim. Cosmochim. Acta* **66**, 1095–1104.

Associate editor: Edwin Schauble